Efficient Visualization and Set-theoretic Difference Operations for Accurate Geometric Modeling in Real-time Simulations

Alexander Leutgeb[a], Michael Florian Hava[b] and Alexander Hans Leitner[c]
Unit Industrial Software Applications, RISC Software GmbH, Softwarepark 35, Hagenberg, Austria

Keywords: Implicit Representation, Point Cloud Fitting, Set-theoretic Modeling, Ray Casting, Real-time Simulation.

Abstract: We present a novel approach, which supports efficient visualization and set-theoretic difference operations for accurate geometric modelling in real-time simulations. The geometric operands can be in any representation as long as they are watertight and are convertible to an oriented point cloud. A novel region growing based fitting routine converts the oriented point clouds into a watertight piecewise quadratic implicit representation. During set-theoretic modeling these implicit representations are mapped to the fixed depth hierarchical grid of the resulting geometric model. Thereby a surface elimination algorithm removes parts not contributing to the final surface. This guarantees that the number of already performed modeling operations have only a minor performance impact on the algorithms processing the model. For visualization a novel ray casting based approach was developed, enabling interactive frame rates at Full-HD screen resolutions. The evaluation of the developed method proves its modeling performance and high geometric accuracy by means of the simulation of subtractive manufacturing examples.

1 INTRODUCTION

There is a strong need for an efficient visualization and set-theoretic difference operations in the context of accurate geometric modeling in real-time simulations. For example, the simulation of subtractive manufacturing - material removal processes, such as milling, turning or drilling - have become complex tasks, requiring efficient systems for their geometric model computation and visualization. The complex multi-axis milling processes result in workpieces with a high-quality surface finish requiring manufacturing tolerances up to 0.001 mm generated by thousands of removal steps.

Conventional solid modeling systems build the foundation for computer-assisted geometric design of "Virtual Products" via Computer Aided Design (CAD) software. These systems are implemented with respect to modeling capabilities, geometric modeling precision, exchangeability of geometric formats between different CAD systems, a geometric representation, which is adequate for further analysis in the fields of Computer-Aided Engineering (Finite-Element-Analysis and Computational-Fluid-Dynamics). Their modeling operations do not offer the necessary performance to support the application in real-time simulations.

Our approach is a geometric modeling system, which supports efficient visualization and set-theoretic difference operations for accurate geometric modelling in real-time simulations. Thereby the number of already performed set-theoretic difference operations has only a minor performance impact on the algorithms processing the geometric model. The obtainable precision of the resulting geometric model matches the requirements of industrial applications. The algorithms of the system utilize the parallelization potential of modern hardware architectures. Summarizing, the novelties introduced in this work are mainly:

- A region growing based fitting routine for oriented points clouds with an implicit representation using piecewise quadratic functions. The resulting representation is watertight.
- A fixed depth hierarchical grid with an efficient elimination strategy during set-theoretic modeling operations.
- An efficient ray casting based visualization supporting interactive frame rates.

[a] https://orcid.org/0000-0001-8934-4501
[b] https://orcid.org/0000-0002-5085-1490
[c] https://orcid.org/0000-0002-4081-2586

Leutgeb, A., Hava, M. and Leitner, A.
Efficient Visualization and Set-theoretic Difference Operations for Accurate Geometric Modeling in Real-time Simulations.
DOI: 10.5220/0008983802990306
In *Proceedings of the 15th International Joint Conference on Computer Vision, Imaging and Computer Graphics Theory and Applications (VISIGRAPP 2020) - Volume 1: GRAPP*, pages 299-306
ISBN: 978-989-758-402-2; ISSN: 2184-4321

2 RELATED WORK

Implicit surfaces are mostly defined by polynomials, of which Quadrics are the most prominent representatives (Menon, 1996). These are polynomials of degree two, which in contrast to polynomials of higher degree, have closed and efficient solutions for certain geometric problems like intersection computations. Distance functions $d(p)$ are special functions from $\mathbb{R}^3$ to $\mathbb{R}$, these compute the distance to the nearest point on the implicit surface defined via $d(p) = 0$ for each point $p \in \mathbb{R}^3$ (Diener, 2012). Signed distance functions (SDF) compute the signed distance, in which negative distances usual represent the inside of an object. In contrast to general implicit functions, distance functions offer several advantages considering the simplicity of several computations, like surface normals (normalized gradient $d(p)$) and set-theoretic operations.

2.1 Discrete Signed Distance Fields

Adaptively sampled distance fields (ADF) use an Octree for hierarchical space decomposition and each cell stores at its eight corner positions the discretized values of a signed distance function (Frisken et al., 2000). The hierarchical subdivision follows the shape of the object according to a defined approximation error. Because of this adaptivity, complex geometric objects can be represented in a memory efficient way. This approach enables an efficient computation of the set-theoretic operations union, intersection, and difference. One prominent method for the visualization of adaptively sampled distance fields is Sphere Tracing. The work of (Bastos and Celes, 2008) represents an efficient implementation on Graphics Processing Units (GPUs).

OpenVDB (Museth, 2013) supports a hierarchical data structure for the efficient representation of sparse, time-varying volumetric data discretized on a 3D grid. These values can be of scalar (signed distance field) or vector (velocity vector field) type. In contrast to an Octree, where the branching factor per dimension is two and its depth determines the precision, OpenVDB uses a tree structure with a fixed depth, and the precision depends on the branching factor per dimension at each hierarchical level. An Octree based approach has a higher memory efficiency because of better adaptivity to the geometric shape, but has higher run-times for searching specific cells and set-theoretic modeling operations. Besides the simulation of time-varying changes of volumes, OpenVDB also supports efficient set-theoretic modeling.

The approaches in this section have the following limitation: In order to reach a high modeling accuracy the size of the leaf cells has to be very fine. This fine granularity has a negative performance impact on set-theoretic modeling operations.

2.2 Continuous Signed Distance Functions

Multi-level partition of unity (MPU) implicits support an adaptive error-driven approximation of a surface via signed distance functions in a precise and fast way (Ohtake et al., 2003). In order to create the implicit representation, the geometric object (in the concrete case defined via an oriented point cloud) is spatial subdivided according to an Octree structure. In each Octree cell a piecewise quadratic function (locale shape function) is created, which approximates the geometry assigned to the according cell. These shape functions behave like signed distance functions and yield a value close to zero in the proximity of the surface of the approximated geometric shape, a positive value inside and a negative value outside. In the case, the local shape function exceeds a defined approximation error for the cell assigned geometric object, the fitting routine subdivides the cell further and performs the approximation on the new child cells. The algorithm repeats this process until the approximation error falls below a defined threshold. Locale shape functions are generic Quadrics, bivariate Quadrics and their set-theoretic combination. By this distinction, it is possible to approximate flat surfaces as well as surfaces with geometric features like corners and edges at a high precision. The usage of signed distance functions enables shape blending, offsetting, and set-theoretic operations like union, intersection, and difference. Visualization methods for MPU implicits are direct rendering in polygonised form or Sphere Tracing (Hart, 1996). Because the MPU approach offers set-theoretic modeling by combining two distinct geometric objects at the time of visualization, it does not scale with increasing number of set-theoretic operations.

Sparse low-degree implicits (SLIM) is a method approximating the surface of a geometric object with surface elements (Surfel) (Ohtake et al., 2005). The geometric object is in form of a point cloud. The definition of a Surfel consists of a sphere (specified via center and radius), and a function approximating the surface inside the sphere. Functions can be linear, quadratic or cubic polynomials. The global surface results from overlapping Surfels and is not continuous. Surface continuity is guaranteed during visualization via ray casting. The construction of the Surfel

representation happens in a hierarchical way, by starting with Surfels with a big radius. Depending on a cost function, which considers the approximation error and memory efficiency the fitting routine further subdivides these Surfels into finer ones. The SLIM approach has the problem, in order to represent geometric features like edges or corners with high geometric accuracy the subdivision of the Surfels must be very fine.

3 GEOMETRIC REPRESENTATION

Our implicit representation is based on the work of (Ohtake et al., 2003) and supports the following kinds of local fitted functions inside a support sphere:

- A bivariate quadratic polynomial in local coordinates.
- A piecewise quadratic surface that fits an edge or a corner.

3.1 Point Cloud Generation

The newly developed geometric modeling method requires a watertight implicit representation of the geometric objects involved in set-theoretic modeling operations. In order to obtain the implicit representation for a given triangle mesh, it is first converted into an oriented point cloud with a specified uniform point density ρ. For each triangle of the input mesh points are generated:

- Triangle vertices: For each triangle vertex a point is generated.
- Triangle edges: If a triangle edge width length l is longer than ρ, then the edge is split into $\lceil l/\rho \rceil$ parts and points are generated between neighbouring parts.
- Triangle area: The longest edge of a triangle forms the base vector. The height vector is orthogonal to the base vector and its magnitude represents the triangle height. The base and height vector form a Cartesian coordinate system, in which an algorithm generates at regular ρ positions points in both dimensions, but only if the point is enclosed by the triangle.

For each generated point the surface normal at its position is computed. Points shared by multiple triangles with different face normals are replicated with the respective normal.

3.2 Overall Fitting Procedure

For the region growing based approximation of the oriented point cloud P the metric $\rho(P)$ is introduced. As the radius of the support sphere during fitting is at least 2ρ, it is guaranteed that the number of points is sufficient for fitting the local shape function.

$$\rho(P) = \max_{a \in P}\left(\min_{b \in P \wedge a \neq b}(\|a-b\|)\right) \quad (1)$$

The region growing approach starts with a seeding phase. Thereby the algorithm chooses a random not already approximated point from the overall point cloud as center for an initial support sphere with radius 4ρ. In the case of a successful fit with a local function, the algorithm shrinks the support sphere with radius r by ρ. The space between the initial and the shrunken sphere is the boundary region (see Figure 1). All points inside the shrunken support sphere are considered as approximated. Now the growing phase begins and the algorithm adds points not already approximated from this boundary region to the set of growing points. Now a new center for a new initial support sphere with radius 4ρ is chosen from this set of growing points. After a successful fit inside the newly created support sphere, the not approximated points from the new bounding region extend the set of the growing points. Points considered as approximated are removed from the set of growing points. Region growing continues until there are no more growing points left. If there are any non-approximated points left, the two stage fitting process starts again.

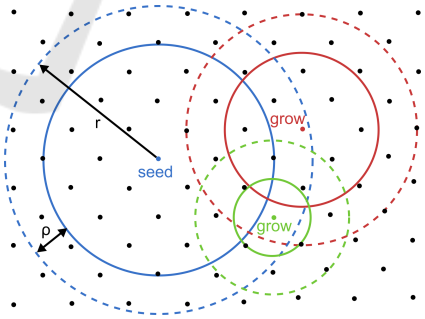

Figure 1: Feeding and growing stages.

For each cluster the fitting with local functions is performed yielding individual bivariate quadratic polynomials. If the approximation error exceeds the defined error threshold, the algorithm shrinks the support sphere by a factor of 0.85 and local function fitting starts again. If the radius gets smaller than 2ρ fitting is not possible at all.

The overall region growing algorithm works in parallel in the following way. First the oriented point

cloud is placed into a regular grid with cell size 4ρ per dimension. The grid is partitioned into n work slices along the dimension with the highest spatial extent, where n is two times the number of logical processors. The minimum slice thickness of two times the cell size prevents race conditions during parallel code execution. The parallel region growing algorithm works in two phases:

- Phase 1: Each logical processor executes the region growing algorithm inside work slices with an even sequence number.
- Phase 2: Each logical process executes the region growing algorithm inside work slices with an odd sequence number.

The result of the algorithm is a watertight approximation of the oriented point cloud with overlapping support spheres and local functions.

4 GEOMETRIC MODELING

4.1 Hierarchical Space Decomposition

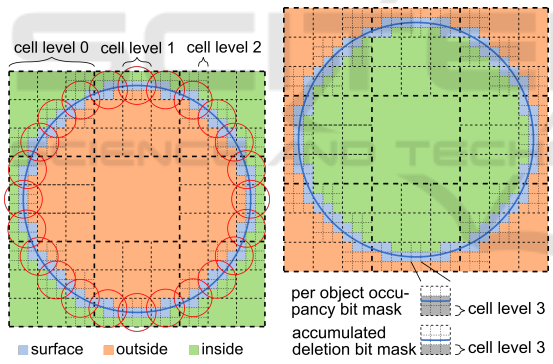

Figure 2: (a) Grid occupancy of first set-theoretic difference operand (support spheres are red and local functions are blue). (b) Modeling grid after set-theoretic difference operation.

During set-theoretic modeling the geometric operand represented by support spheres with their local functions is mapped to a hierarchical grid with a fixed depth (see Figure 2). The developed space-partitioning scheme is similar to OpenVDB (Museth, 2013) and shares the same advantages (see section 2.1). The cells of the grid can have the classifications inside, outside or surface. By convention the initial geometric object is considered as the first set-theoretic difference operand and therefore its surface orientation is inverted (see Figure 2 (a)) and the initial modeling grid is completely inside. Surface classification can only occur on cell level 2, whereas the classifications inside and outside can also occur on higher cell levels. The mapping of the surface represented via the support spheres with their local functions to cells works as following. The algorithm checks each support sphere if it overlaps with cells at cell level 0. If this is the case, it checks the overlap for each child cell at the next cell level. It repeats this procedure until cell level 2 is reached. Section 4.2 explains checking for actual surface contribution of a support sphere with its local function on cell level 2. The finest cell level 3 stores a per geometric object grid occupancy bit mask and an accumulated deletion bit mask. The mapping logic for cell level 3 is the same as for cell level 2. Section 4.3 explains the usage of cell level 3 in the context of surface elimination.

4.2 Cell Classification

Surface Cells. A support sphere and its local function are only assigned to a cell on level 2, if there actually is a surface contribution inside the cell. The surface contribution is computed in the following way. At first the algorithm computes the axis aligned bounding box (overlap box) resulting from the overlap between the support sphere and the cell. If the function has a surface contribution inside the cell it must cross at least one of the six faces of the overlap box. In Figure 3 you see one face of the overlap box colored green. The red circle marks the intersection between the support sphere and a face plane. The blue curve marks the intersection between the local function and the face plane. The green filled circles mark the positions, where the signed distance function is evaluated, and contain the sign of the value. In the case this position is outside the support sphere, the green filled circles are empty. In Figure 3 (a) to (c) you see the recursive subdivision scheme of the algorithm, which stops depending on the following cases:

- There are sign changes between neighboring evaluation points so the function crosses the space between these two points and we have a surface contribution inside the cell. The reference point (filled red circle) is the intersection between a line ranging between these two points and the local function.
- The size in both dimensions of the subdivided rectangular areas falls under a certain threshold so no surface contribution was detected.

The reference point is needed for inside/outside calculation during visualization via ray casting (see section 5.2).

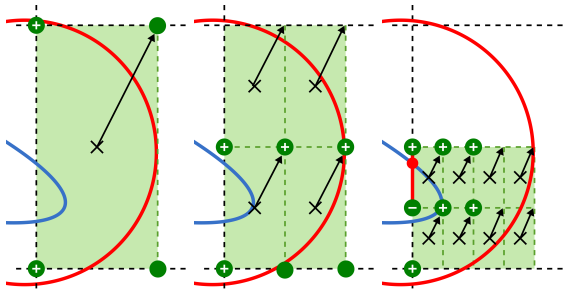

(a) (b) (c)

Figure 3: Determination of surface contribution for local function. (a) Initial area. (b) Areas after first subdivision. (c) Areas after second subdivision.

Inside/Outside Cells. The classification algorithm categorizes the non-surface cells into inside or outside cells in the following three ways, sorted by increasing computational costs:

1. Adopt the classification of direct neighboring cell.
2. If cell center is inside a support sphere evaluate the according signed distance function for the position and derive classification from sign of result.
3. If cell center is outside of any support sphere, create a line ranging from the cell center to the center of the closest support sphere. Compute the intersection point between the line and the support sphere. Evaluate signed distance function for intersection position and derive classification from sign of result.

4.3 Surface Elimination

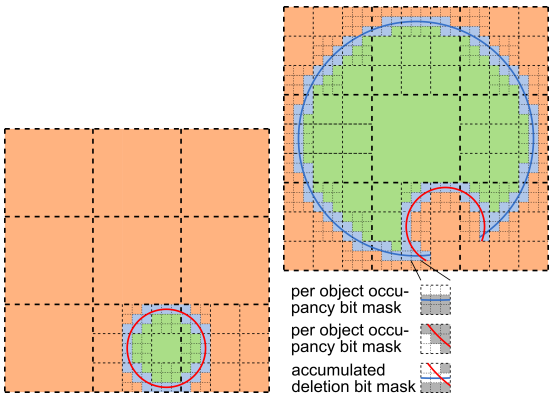

(a) (b)

Figure 4: (a) Grid occupancy of second set-theoretic difference operand. (b) Modeling grid after set-theoretic difference operation showing surface elimination.

Figure 4 illustrates the process of surface elimination. (a) shows the grid occupancy of the second set-theoretic difference operand. In (b) you see the modeling grid after the set-theoretic difference operation, where all the surface cells of the initial geometric object inside the surface cells of the set-theoretic difference operand were cleared. Clearing in this context means removing all surfaces from surface cells and changing the cell classification from surface to outside. If all child cells of a parent cell have the same cell classification outside, then the subdivision of the parent cell into child cells is withdrawn and the algorithm transfers the child cell classification to the parent cell. Additional surface elimination can occur by using the information from cell level 3. Thereby we have to differentiate between two different cases:

- If all the bits in the accumulated deletion bit mask are set, then all surfaces from the surface cell are removed and the cell classification is changed to outside.
- If for all the set bits of the per object occupancy bit mask the according bits in the accumulated deletion bit mask are set, then the surface of the geometric object can be removed.

5 VISUALIZATION

5.1 Ray Casting of Watertight Surfaces

For the visualization of surfaces resulting from set-theoretic modeling ray casting was first mentioned in the work of (Roth, 1982). Thereby the operands involved during modeling must be in watertight form. The basic idea is to calculate the surface intersections of all involved geometrics objects with the ray. Then the algorithm sorts the intersections according to an increasing distance between ray origin and intersections. Now the algorithm calculates the resulting surface point in the following way. It starts with a counter initialized with a predefined value. By going through the list of intersections it decrements or increments this counter depending on the fact if a ray enters respectively leaves a geometric object at the current intersection. The method detects entering or leaving by using the surface normal at the intersection point and the normalized ray direction. If the normalized ray direction points into the same half-space as the surface normal the ray leaves the geometric object, otherwise the ray enters it. If during counting the counter reaches a defined value the resulting surface point is hit. This visualization principle is also applicable to the developed surface representation, because overlapping support spheres with local functions describe a watertight surface of a geometric operand.

5.2 Ray Casting of Non-watertight Surfaces

Because of the surface elimination during set-theoretic modeling we lose the watertightness of the geometric operands. In Figure 5 (a) you see the grid occupancy in the case of a set-theoretic difference operation where the initial geometry is colored blue and the subtractive geometry is colored green. By convention, we define the initial geometric object as first subtractive geometric object. Therefore the counter at the ray origin is initialized with -1 (ray origin inside initial geometric object). During counting, the algorithm reaches the resulting surface point, if the counter gets the value 0. If we execute the usual counting procedure, the resulting surface point will be wrong, because of the missing ray intersections between the ray and the geometric objects.

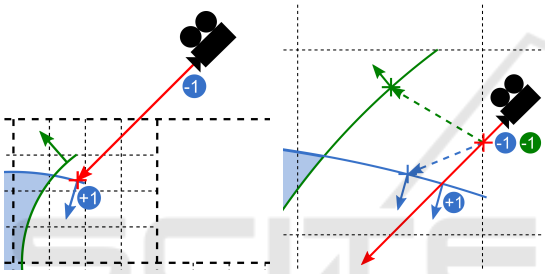

Figure 5: (a) Wrong resulting surface point (red cross) during counting. (b) Calculating the number of geometric objects containing the entry point (red cross) and surface point evaluation via counting.

The solution to this problem is to perform the counting procedure not globally but locally on surface cell level. Therefor we must first reconstruct the missing ray entries for all geometric objects inside a surface cell (see Figure 5 (b)). That means the algorithm calculates the point, where the ray enters the surface cell (entry point). Then it calculates the number of geometric objects containing the entry point. Therefor it builds for each geometric object a secondary ray ranging from the entry point to the reference point on the surface of the geometric object. It computes all intersections between the secondary ray and the piecewise surfaces of the geometric object and determines the closest intersection to the entry point. For the closest intersection, the procedure computes the surface normal via the gradient of the according local function. If this surface normal and the secondary ray direction point into the same half-space, the entry point is inside the geometric object. After the computation of the number of geometric objects containing the entry point, the algorithm initializes the counter with its negative value. Then it computes the intersections between the ray and the surfaces of the geometrics objects. These intersections are again sorted according to an increasing distance between ray origin and intersection. By going through the list of intersections the procedure decrements or increments this counter as usual. If the counter gets to 0, the algorithm reached the resulting surface point.

5.3 Acceleration Structure and Coherent Ray Traversal

For ray casting a two level hierarchical grid is used with matching positions between level 2 cells of the modeling grid and leaf cells of the ray casting grid. Usually in ray-casting spatial decomposition techniques follow the shape of the geometric objects (e.g. Bounding Volume Hierarchies and kd-Trees). The developed approach subdivides space at fixed boundary positions, because of the surface elimination strategy. The work of (Wald et al., 2009) gives an overview of the different spatial decomposition techniques in the context of ray casting.

This two level grid approach offers a good compromise between traversal time, actual surface evaluation time inside cells, and sparsity. Based on the work of (Kalojanov et al., 2011) we expect this design to be adequate for a future implementation for Graphics Processing Units (GPUs). During ray casting the rays for the whole screen resolution are organized in coherent ray packets traversing the two level grid slice by slice. Neighboring rays inside a ray packet mostly traverse the same cells so the algorithm benefits from the induced memory coherence. A packet size of 4x4 rays turned out to be the most performant for the overall ray-casting procedure. The work of (Wald et al., 2006) gives an introduction into ray casting of scenes with coherent grid traversal, comparing the visualization times for different ray packet sizes.

During ray-casting we intersect each cell of the traversed slices with the rays of the ray packet. The algorithm marks the rays, which have already intersected the resulting surface, as inactive. The remaining active rays are compacted for vectorized processing. Depending on the number of active rays intersecting a cell the algorithm branches in a vectorized or scalar processing intersection routine. In the current implementation, the threshold for vectorized processing is at least 4 rays intersecting a cell. By using Central Processing Units (CPUs) at least with Streaming SIMD Extension 4 (SSE4) support, we can perform 4 single precision floating point calculations in parallel at CPU core level.

6 EVALUATION

The experimental results presented in this section are based on the following hardware configuration: Intel Xeon E5-1660 v4 (eight cores @ 3.4 GHz [Turbo], theoretical peak performance 435.2 GFlops in single precision) and 32 GB DDR4 2400 RAM. For evaluation, we are using a static grid configuration of 20 cells per dimension at level 0, 5 at level 1, 5 at level 2 and 3 at level 3. All renderings were performed with a resolution of 1920 x 1080. The point clouds of the geometric operands were fitted with a geometric approximation error of 0.01 % of the maximal spatial model extent.

Comparing to Related Work. To compare our method with the approaches (MPU, 2003) and (SLIM, 2005) we use two different geometric modeling examples based on subtractive manufacturing processes, see Figure 6 and Table 1. Note that only our approach is parallelized, therefore a speedup of up to factor 8 is to be expected.

(a) Impeller (b) Gear

Figure 6: Resulting geometric objects.

Table 1: Point cloud size of initial and subtractive objects.

Example	Initial	Subtractive
Impeller	536959	19896
Gear	263854	44120

Table 2 and Table 3 summarize the measured times in milliseconds for fitting and rendering of one frame. As the MPU and SLIM implementations do not make use of parallel code exeuction, we provide single-threaded measurements (Our_{ser}) in addition to multi-threaded ones (Our_{par}). Given the non-embarrassingly parallel nature of overall fitting we cannot achieve the theoretical maximum speedup, yet still outperform the single threaded alternatives in all but one test. Even if we switch to serial execution our approach to rendering outperforms the alternatives due to conceptual differences.

Table 2: Comparison of fitting times in milliseconds.

Example	MPU	SLIM	Our_{ser}	Our_{par}
$Imp._{init}$	6300	107711	13684	1369
$Imp._{sub}$	870	1720	2541	751
$Gear_{init}$	4339	51423	6870	1061
$Gear_{sub}$	2671	2158	9130	2925

Table 3: Comparison of rendering times in milliseconds.

Example	MPU	SLIM	Our_{ser}	Our_{par}
$Imp._{init}$	15930	1750	778	125
$Imp._{sub}$	6548	510	394	112
$Gear_{init}$	16923	870	406	90
$Gear_{sub}$	26311	1570	1308	270

Benchmarking of Geometric Modeling Examples. In both of these examples the simulation starts with an initial geometry and consecutively applies set-theoretic difference operations. The measured modeling times vary considerably depending on the amount of cells affected by the respective operation. The number of already completed modeling steps has only negligible impact (see Figure 7).

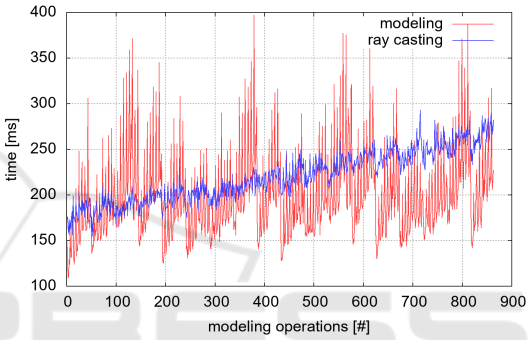

(a) Impeller

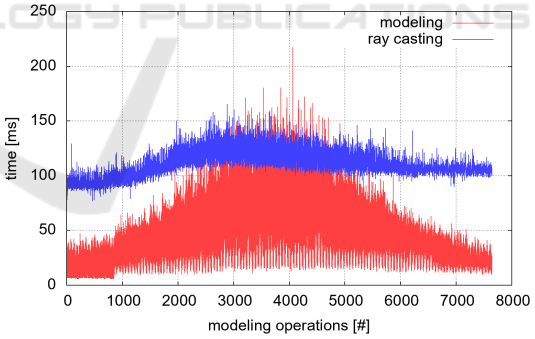

(b) Gear

Figure 7: Measured times for modeling and visualization of one frame.

Analyzing the rendering performance, one can see that the number of already completed modeling operations only marginally impacts our visualization approach. Figure 6 presents the resulting geometric objects after the completion of all modeling operations from the perspective used for the visualization benchmarking. Even though modeling in example *Impeller* affects large parts in image space and rendering times are bound to rise, there is only moderate growth in rendering time. In example *Gear* the rendering times

stay almost constant, because only very small parts in image space are affected by the overall modeling.

7 CONCLUSIONS

The experimental results have proven that our approach is proper for precise geometric modeling in real-time simulations. The number of already completed modeling operations has only a minor performance impact on the algorithms processing the geometric model, provided the surface elimination works in an efficient way. Currently the surface elimination algorithm uses as smallest elimination granularity the cells of the hierarchical modeling grid at the finest level. A cell is marked for deletion, if it is completely covered by a geometric modeling operand. A future extension to the elimination strategy is the detection of complete containment of one geometric operand in another one on surface cell level, which is not limited by fixed spatial boundaries. Some additional points for future improvements are:

- The visualization routine would benefit from an implementation for Graphics Processing Units (GPUs), due to the embarrassingly parallel problem formulation of ray casting.
- Introduction of set theoretic union operation requiring an extension to the surface elimination and visualization strategy.

ACKNOWLEDGEMENTS

This project is co-financed by the European Fund for Regional Development (EFRE) and the state of Upper Austria as part of the program “Investing in Growth and Jobs” (IWB). Further information can be found on https://www.iwb2020.at.

REFERENCES

Bastos, T. and Celes, W. (2008). Gpu-accelerated adaptively sampled distance fields. In *2008 IEEE International Conference on Shape Modeling and Applications*, pages 171–178.

Diener, C. L. (2012). Procedural modeling with signed distance functions. Unpublished bachelor’s thesis, Karlsruher Institute of Technology, Karlsruhe, Germany.

Frisken, S. F., Perry, R. N., Rockwood, A. P., and Jones, T. R. (2000). Adaptively sampled distance fields: A general representation of shape for computer graphics. In *Proceedings of the 27th Annual Conference on Computer Graphics and Interactive Techniques*, SIGGRAPH ’00, pages 249–254, New York, NY, USA. ACM Press/Addison-Wesley Publishing Co.

Hart, J. C. (1996). Sphere tracing: a geometric method for the antialiased ray tracing of implicit surfaces. *The Visual Computer*, 12(10):527–545.

Kalojanov, J., Billeter, M., and Slusallek, P. (2011). Two-level grids for ray tracing on gpus. *Computer Graphics Forum*, 30(2):307–314.

Menon, J. (1996). An introduction to implicit techniques. In *Course Notes of the 23rd Annual Conference on Computer Graphics and Interactive Techniques - Implicit Surfaces for Geometric Modeling and Computer Graphics*, pages 13–26, New Orleans, LA, USA.

MPU (2003). Mpu software. http://home.eps.hw.ac.uk/~ab226/software/mpu_implicits/mpu/mpu_oct_03.zip. Retrieved July 7, 2016, from Heriot Watt University.

Museth, K. (2013). Vdb: High-resolution sparse volumes with dynamic topology. *ACM Trans. Graph.*, 32(3):27:1–27:22.

Ohtake, Y., Belyaev, A., and Alexa, M. (2005). Sparse low-degree implicit surfaces with applications to high quality rendering, feature extraction, and smoothing. In *Proceedings of the Third Eurographics Symposium on Geometry Processing*, SGP ’05, Aire-la-Ville, Switzerland, Switzerland. Eurographics Association.

Ohtake, Y., Belyaev, A., Alexa, M., Alexa, M., Turk, G., and Seidel, H.-P. (2003). Multi-level partition of unity implicits. *ACM Trans. Graph.*, 22(3):463–470.

Roth, S. D. (1982). Ray casting for modeling solids. *Computer Graphics and Image Processing*, 18(2):109 – 144.

SLIM (2005). Slim software. http://www.riken.go.jp/lab-www/VCAD/VCAD-Team/members/ohtake/slim/. Retrieved July 7, 2016, from RIKEN.

Wald, I., Ize, T., Kensler, A., Knoll, A., and Parker, S. G. (2006). Ray tracing animated scenes using coherent grid traversal. *ACM Trans. Graph.*, 25(3):485–493.

Wald, I., Mark, W. R., Günther, J., Boulos, S., Ize, T., Hunt, W., Parker, S. G., and Shirley, P. (2009). State of the art in ray tracing animated scenes. *Computer Graphics Forum*, 28(6):1691–1722.